Searching for Radiative Hydrodynamic Instabilities in the Envelopes of Massive Stars

Shangfei Liu[1], Richard Stancliffe[2], Matthias Gritschneder[3], Mark Krumholz[4]

liushangfei@pku.edu.cn, gritschneder@kiaa.pku.edu.cn,
Richard.Stancliffe@sci.monash.edu.au, krumholz@ucolick.org

ABSTRACT

We investigate local radiative hydrodynamic instabilities in the envelopes of massive stars. Two different stellar models are considered, a simple polytropic model and a more realistic stellar evolution code model. For both cases, we compare the local optical depth and radiative flux with analytically derived instability criteria. Only a thin outer shell of the star, containing a mass of about $10^{-6} M_\odot$ to $10^{-5} M_\odot$, can be subjected to this instability. However, the growth rate of the instability is relatively fast ($\sim 10^4$ s) indicating a possible run-away effect.

Subject headings: massive stars — radiative hydrodynamic instabilities

1. Introduction

Massive stars are still enigmatic in different evolutionary stages. It is yet unclear how massive stars form, e.g. by core accretion or by competitive accretion (Krumholz & Bonnell 2009). The Eddington limit predicts that there should be an upper limit of stellar mass. If a star grows beyond that limit, the radiation pressure becomes so strong that it will blow away the outer part of the stellar envelope. Figer (2005) did find an absence of stars with masses greater than $130 M_\odot$ in the Arches cluster, and therefore claimed that this upper limit is $150 M_\odot$, which has been widely accepted. However, a very recent observation shows

---

[1]Department of Astronomy, Peking University, Beijing 100871, China

[2]Centre for Stellar and Planetary Astrophysics, School of Mathematics, Monash University, Clayton VIC 3800, Australia

[3]Kavli Institute for Astronomy & Astrophysics, Peking University, Beijing 100871, China

[4]Department of Astronomy & Astrophysics, University of California, Santa Cruz, CA 95064, U.S.A.

that several young stars in the R136 star cluster exceed that limit. One of them might have a mass as high as $320M_\odot$ (Crowther et al. 2010). It is natural to ask whether these super massive stars are stable or not.

Luminous blue variables (LBVs) are very massive, luminous evolved stars characterized by long term variability and occasional eruptions with substantial mass loss. η Carinae, one of the most spectacular LBVs, is well known for its great eruption around 1843, when it produced the total luminous energy as much as a supernova does but survived (Davidson & Humphreys 1997). Several scenarios to explain such a supernova impostor have been proposed, but uncertainties still remain. Using high-resolution far ultraviolet spectra Iping et al. (2005) confirmed that η Carinae is a close binary system, which has already been inferred from the 5.52 year variability period (Damineli 1996). Some authors argued that the great eruption was due to the binary evolution, either a close encounter (Kashi & Soker 2010) or a collision (Smith 2010). However, since almost all LBVs are single stars (Vink 2009), the binary evolution scenarios may not account for all the supernovae impostor events.

We will focus on investigating the possibilities of local radiative instabilities inside the envelopes of massive main sequence stars, which may give a hint on understanding the abnormal behaviors of massive stars. This report is organized as follows. In §2 we describe our basic formalism and derive the instability criteria in the short-wavelength limit under radiative diffusion assumption. In §3 we introduce two stellar models, the polytropic model as well as the stellar evolution code model. In §4 we present the results of our calculations using the two different criteria and briefly discuss them. The summary is given in §5.

2. Dispertion Ralation and Stability Analysis

2.1. Basic Equations and Assumptions

Here we adopt the eqations of radiation magnetohydrodynamics and their notations discussed by Blaes & Socrates (2003, hereafter BS03) and references therein. As a first step we neglect the magnetic field to simplify the equations, so the basic fluid equations are

$$\frac{\partial \rho}{\partial t} + \boldsymbol{\nabla} \cdot (\rho \boldsymbol{v}) = 0, \tag{1}$$

$$0 = -\boldsymbol{\nabla} p + \rho \boldsymbol{g} + \frac{\kappa_F \rho}{c} \boldsymbol{F}, \tag{2}$$

$$\frac{\partial u}{\partial t} + \boldsymbol{v} \cdot \boldsymbol{\nabla} u + \gamma u \boldsymbol{\nabla} \cdot \boldsymbol{v} = \kappa_J \rho c E - \kappa_P \rho c a T_g^4 - \kappa_T \rho c \left(\frac{4 k_B T_g}{m_e c^2} - \frac{h\bar{\nu}}{m_e c^2} \right) E, \tag{3}$$

$$\frac{\partial E}{\partial t} + \boldsymbol{v} \cdot \boldsymbol{\nabla} E + \frac{4}{3} E \boldsymbol{\nabla} \cdot \boldsymbol{v} = -\kappa_J \rho c E + \kappa_P \rho c a T_g^4 + \kappa_T \rho c \left(\frac{4 k_B T_g}{m_e c^2} - \frac{h\bar{\nu}}{m_e c^2} \right) E, \qquad (4)$$

$$\frac{1}{3} \nabla E + \frac{\kappa_F \rho}{c} \boldsymbol{F} = 0, \qquad (5)$$

where ρ, p, T_g, T_r, u, E are the density, pressure, gas temperature, radiation temperature, energy density in the gas and radiation energy density, repectively. The relations between these quantities are

$$\mu = \frac{p}{\gamma - 1}, \qquad (6)$$

$$p = \frac{\rho k_B T_g}{\mu}, \qquad (7)$$

$$E = a T_r^4, \qquad (8)$$

where γ is the ratio of specific heats in the gas, and μ is the mean molecular weight of the gas. These two quantities are assumed to be constant in the following discussions. T_g and T_r are gas and raidation temperatures, respectively. $\kappa_J, \kappa_P, \kappa_F$ and κ_T are opacities defined by different weighting functions which are denoted under the subscripts (angle-averaged mean specific intensity, Planck function, radiation flux and Thomson scattering, respectively). Other constants are: c is the speed of light, a is the radiation density constant, k_B is Boltzmann's constant, and m_e is the electron mass. The vector $\boldsymbol{v}$ is the fluid velocity, and $\boldsymbol{g}$ is the gravitational acceleration, which is assumed to be time independent.

As mentioned in BS03, we only consider static equilibria in LTE, which means the equilibrium fluid velocity is zero and gas temperature and radiation temperature are tightly coupled

$$T_g = T_r \equiv T. \qquad (9)$$

We assume radiative equilibrium

$$0 = \boldsymbol{\nabla} \cdot \boldsymbol{F}, \qquad (10)$$

which is already used to derive Equation (5).

2.2. Hydrodynamic Instabilities within Short-Wavelength Limit and $T_g = T_r$

By adopting a linear perturbation in total pressure (gas plus radiation), BS03 derives an equation for the total pressure perturbation in terms of the density and velocity perturbations, which is equation (40) in BS03. Combining the perturbation equation with perturbed continuity equation, perturbed gas momentum equation and flux freezing equation, they get a dispersion relation for short-wavelength modes on a static, stratfied, and magnetized equilibrium (equation (49)).

In this work we will not use the eight-mode dispersion relation directly, because it's too complicated for our simple stellar models and as mentioned before we have to assume some simplifications, so that numerical computations are possible. At this stage, we suppose magnetic effects are not prominent. In the short-wavelength limit with $T_g = T_r$, the dispersion relation then reduces to four modes (cf equation (59) in BS03). Here we are only interested in the acoustic wave modes. We take the equation (62) in BS03, which is the first-order corrections to the frequencies of acoustic waves:

$$\omega = \pm k c_i - i\frac{\kappa_F}{2cc_i}\left(1 + \frac{3p}{4E}\right)\left[\left(\frac{4E}{3} + p\right)c_i \mp \left(\hat{\mathbf{k}} \cdot \mathbf{F}\right)\Theta_\rho\right] + \mathcal{O}(k^{-1}), \tag{11}$$

where

$$c_i \equiv \left(\frac{p}{\rho}\right)^{1/2} \tag{12}$$

is the isothermal sound speed in the gas and Θ_ρ is logarithmic derivative of the flux mean opacity κ_F with respect to the density:

$$\Theta_\rho \equiv \frac{\partial \ln \kappa_F}{\partial \ln \rho} > 0. \tag{13}$$

We use isothermal sound speed in equation (11) because gas and radiation temperatures are assumed to be tightly coupled.

Note that we have adopted wave form like $\exp[i(\mathbf{k} \cdot \mathbf{r} - \omega t)]$, so the acoustic waves become unstable if the right-hand side of equation (11) has positive imaginary part, which corresponds to the second term within the brackets (equilibrium flux F) dominates the first term (damping by radiative diffusion). One can easily find that if we take the upper sign of right-hand side of equation (11), the upward-propagating wave is unstable. While taking the lower sign of right-hand side of equation (11), $\hat{\mathbf{k}}$ is negative, then the imaginary part will be positive. However, the real part $\omega = -kc_i$ becomes negative, which means the waves propagate in the opposite direction of $\hat{\mathbf{k}}$ corresponding to upward-propagating waves. So we conclude that only the upward-propagating wave is unstable.

If we assume $\hat{\mathbf{k}}$ and $\mathbf{F}$ to be parallel, the instability criterion for the upward-propagating wave could be simplified as

$$F\Theta_\rho \gtrsim \left(\frac{4E}{3} + p\right)c_i, \tag{14}$$

and an order-of-magnitude estimate would be

$$F\Theta_\rho \gtrsim \max[E, p]c_i. \tag{15}$$

In this work we are considering massive stars, where the radiation pressure E dominates gas pressure p in the stellar envelopes, so equation (15) becomes $F\Theta_\rho \gtrsim Ec_i$. Radiative diffusion

assumption implies that $F \sim Ec/\tau_\mathrm{F}$, where τ_F is the flux mean (Rosseland) optical depth, so equation (15) can be written as

$$\tau_\mathrm{F} \lesssim \left(\frac{c}{c_\mathrm{i}}\right) \Theta_\rho. \tag{16}$$

3. Hydrodynamic Instabilities Check with Different Stellar Models

3.1. n=3 Polytropic Stellar Model

As a first order approximation we investigate the problem with a simple toy model (e.g. a polytropic stellar model). We use the approach discussed in chapter 19 of Kippenhahn & Weigert (1994). By assuming a polytropic index $n = 3$, the polytropic relation between pressure and density of the star is given as:

$$P = K\rho^{\frac{4}{3}}, \tag{17}$$

where $K = \pi G\rho_c^{2/3}R^2/z_3^2$ is the polytropic constant, $G = 6.673 \times 10^{-8}$ dyn cm^2 g^{-2} is the gravitational constant, and $z_3 \simeq 6.897$ defines the surface of the polytrope of index 3. The central density of the star ρ_c can be determined by the mass M and radius R of the star:

$$\rho_c = 54.18\frac{3M}{4\pi R^3}. \tag{18}$$

We can get the density profile from

$$\rho(r) = \rho_c w^3, \tag{19}$$

where w is the solution of the third order Lane-Emden equation $w'' + 2w'/z + w^3 = 0$. The pressure can then be calculated from equation (17). If we assume the ratio $\beta = P_{gas}/P$ is constant throughout the star, we can obtain the value of β from "Eddington's quartic equation":

$$\frac{1 - \beta}{\mu^4\beta^4} = 3.02 \times 10^{-3} \left(\frac{M}{M_\odot}\right)^2, \tag{20}$$

where μ is the mean molecular weight. For an ideal gas with radiation pressure, the temperature can be derived from

$$P = \frac{R}{\mu}\rho T + \frac{aT^4}{3} = \frac{R}{\mu\beta}\rho T, \tag{21}$$

where $R = 8.31 \times 10^7$ erg K^{-1} mol^{-1} is the universal gas constant. Thus, given the mass, radius and chemical compostion of a star, the thermal quantities can be derived by the above equations.

We use equation (16) to check the instabilities. τ_F can be estimated using

$$\tau_F \simeq \kappa \cdot \rho \cdot \left(\frac{\rho}{d\rho/dr} \right), \tag{22}$$

where the Rosseland mean opacity κ is taken from an opacity table for solar metallicity and is based on the local temperature and density (cf section 3.2).

3.2. Stellar Evolution Code

The stellar evolution code STARS was originally developed by Eggleton (1971) and substantial modifications have been made since then[1]. The most recent update was done by Stancliffe & Eldridge (2009), which includes some new features such as binary evolution and stellar mass loss. STARS uses an one-dimensional Lagrangian approach to compute the stellar structure and chemical evolution simultaneously, iterating all variables at the same time to converge to a new model.

To get a model of a massive star, we add mass to an existing less massive stellar model of zero-age main sequence (ZAMS) slow enough to allow it to converge. We iterate this process keeping the model not evolving until it reach the desired mass. In this way, we produce several typical massive stellar models. In addition, we could produce more models to study the trends in the future.

The code deals with a wide range of metallicities by using different opacity tables from $Z = 0$ to $Z = 0.05$ (Stancliffe & Eldridge 2009). In this work, we assume that all the stars have solar chemical abundance, which corresponds to $Z = 0.02$, initially. Figure 1 shows how the opacities varies with densities and temperatures for solar metallicity (the density has been scaled by the temperature in 10^6K). The blue solid line represents the Rosseland mean opacities of a $300M_\odot$ stellar model computed by the code. Note that due to the interior nucleosynthesis, the central metallicity would be a little bit higher than the inital value $Z = 0.02$. The stellar evolution code automatically handles the changes of chemical abundance (e.g. carbon and oxygen enrichment) and computes the real opacities properly. Therefore, the high temperature end of the curve, which represents the the center of a star, is not exactly on the original opacity plane. However, the deviation is rather small (note the slight difference between cyan dotted line and orange solid line in figure 2), and does not affect the results of the instability analyses. Thus, we can use the opacity table for $Z = 0.02$ in polytropic stellar models in spite of the changes of chemical composition. Furthermore,
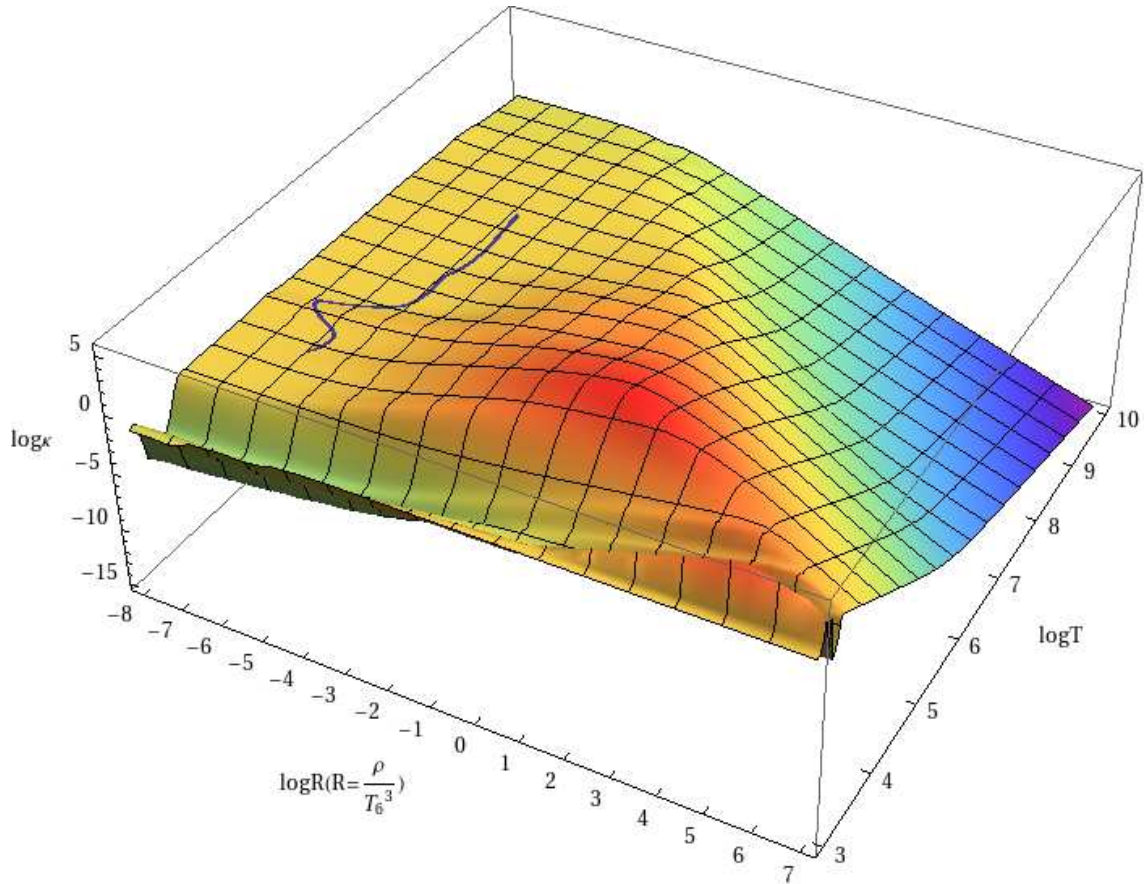
---

[1]See STARS's website: http://www.ast.cam.ac.uk/~stars/

Fig. 1.— The Rosseland mean of the opacity κ (in cm^2 g^{-1}) as a function of T (in K) and $R = \rho/T_6^3$ (in g cm^{-3}) for solar chemical abundance, where $T_6 = T/10^6$K. The blue solid line indicates a $300 M_\odot$ stellar model.

the result can be compared with that of the stellar evolution code, since the difference is caused by the models themselves not by the methods by which the opacities are calculated.

4. Results

First we use equation (16) to perform the instability check for the $85 M_\odot$, $150 M_\odot$ and $300 M_\odot$ stellar models, repectively. Figure 3 shows the results of comparison: the green dotted lines and blue solid lines describe the local values of the optical depth and the instability criterion given by the right-hand side of euqation (16) for polytropic models, while red dashed lines and cyan dashed lines are the local values of optical depth and the instability criterion for the STARS models.
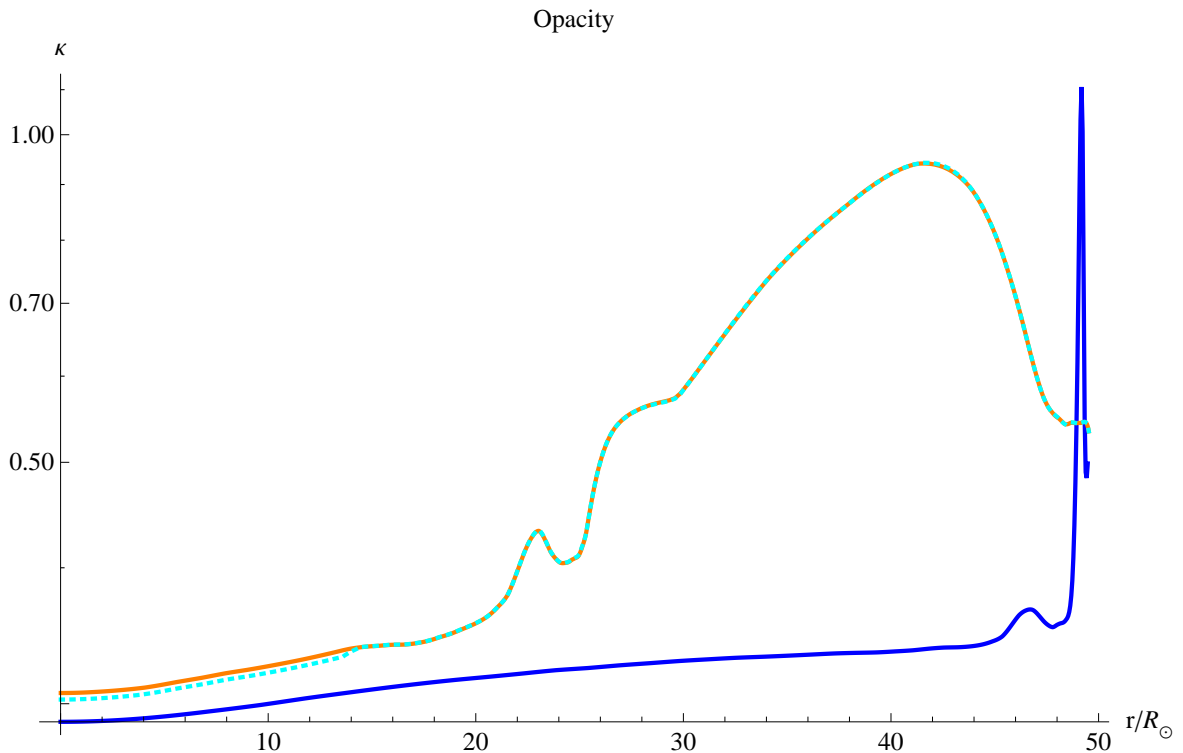
Opacity

Fig. 2.— Different opacities of 300 $M_\odot$ stellar models. The blue solid line is calculated by looking up the opacity table using the temperatures and densities of an n=3 polytropic stellar model. The orange solid line is also obtained by looking up the opacity table but using temperatures and densities of a STARS model, while the cyan dotted line is using the opacities directly calculated in the code.

We find that the optical depth could drop below the threshold of unstable optical depth near the stellar surface in every model, which means that the short-wavelength acoustic waves may become unstable in that regions. However, this conclusion is weakened by two facts: 1) the polytropic model may not be a good approximation when the stars become very massive: the difference of opacities between the polytropic model and the STARS model is large in figure 2; 2) The method of estimating optical depth may not be correct at some points: equation (22) to some negative values in the STARS models, so the lines of optical depth in logarithmic scale become discontinuous in figure 3.

Figure 4 shows the results of using equation (14) to perform the instability check for 85 $M_\odot$, 150 $M_\odot$ and 300 $M_\odot$, respectively. The orange dashed lines represent the radiative flux, and the green dashed lines represent the energy density propagating at the sound speed. Again, the radiative flux can overtake the energy damping near the stellar surface, which means that the radiative flux accumulates the local energy density faster than the acoustic

waves could transport the energy density upward. Figure 4 also suggests that massive stars more likely satisfy this criterion. Our calculations show that only $10^{-6}M_\odot$ to $10^{-5}M_\odot$ are subject to the instability because of the low density in the outer envelopes of massive stars. As the growth rate of the instability is higher than 10^{-5} s^{-1}, even a tiny unstable layer may lead to a global eruption.

5.   Conclusions & Discussion

We apply the instability analysis of BS03 in the context of the envelopes of massive stars, where the radiation pressure dominates the gas pressure. The massive stars are modeled using a $n = 3$ polytropic model and a more realistic model calculated by a stellar evolution code (STARS). For a first estimate, we compare the optical depth and the instability threshold in each stellar model for $85M_\odot$, $150M_\odot$ and $300M_\odot$, respectively. The short-wavelength acoustic waves in the regions where the optical depth drops below the instability threshold are potentially unstable.

We also check the instability in the STARS model by comparing the speeds of radiative flux and radiative damping. The results are similar to those of the simple estimation by the optical depth. We do see these unstable regions near the stellar surfaces, where the radiative flux accumulates the local radiation energy density faster than the radiative damping at the sound speed in the gas. The more massive the star is, the further inwards it will become unstable. Although the masses of the unstable layer are not substantial, the growth rate is relatively short, which may lead to a run away effect.
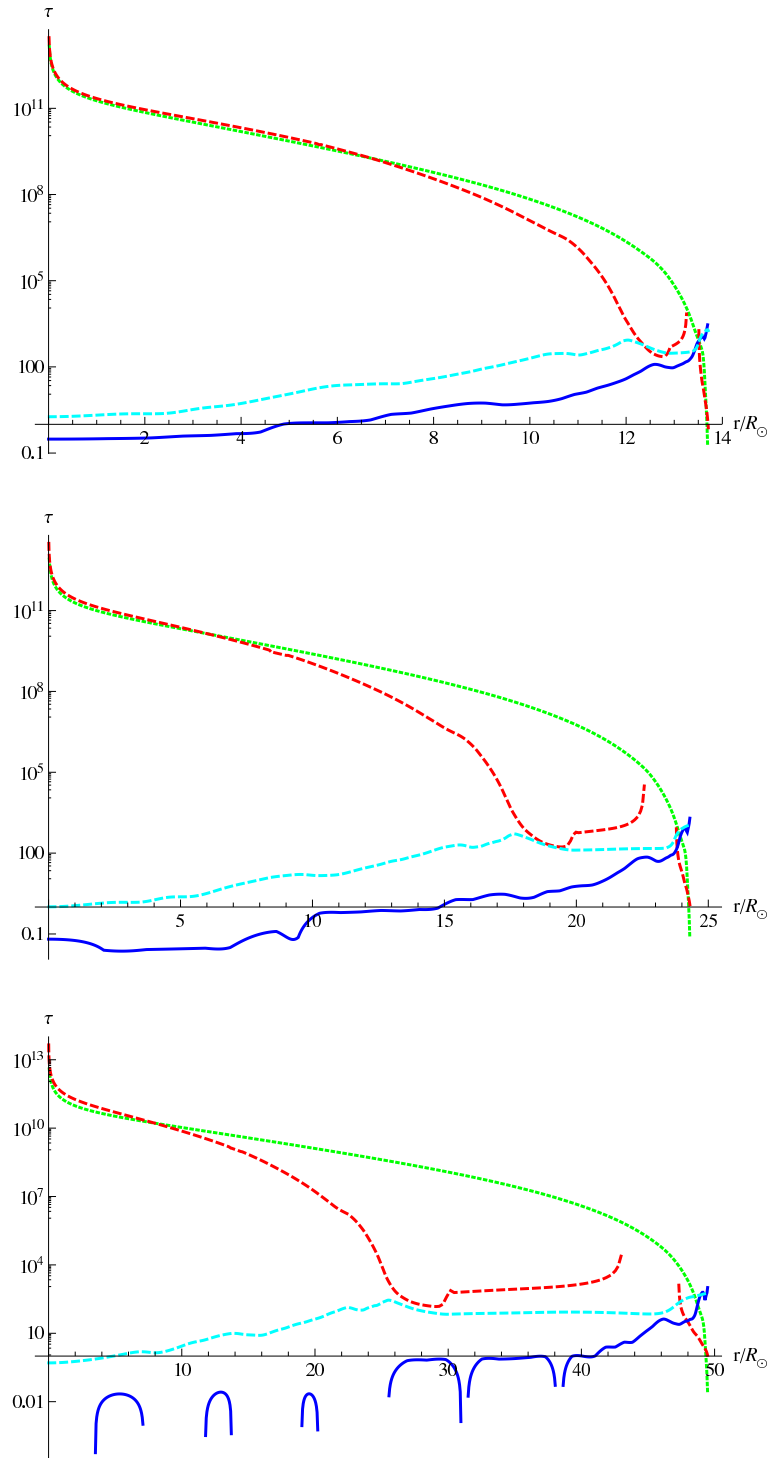
Fig. 3.— Optical depth vs. Threshold of instability criterion. From the top to the bottom are 85 $M_\odot$, 150 $M_\odot$ and 300 $M_\odot$, respectively. Green solid lines and blue solid lines are the optical depth and the threshold of instability criterion in each polytropic model, while red dashed lines and cyan dashed lines are the optical depth and the threshold of instability criterion in each STAR's model.
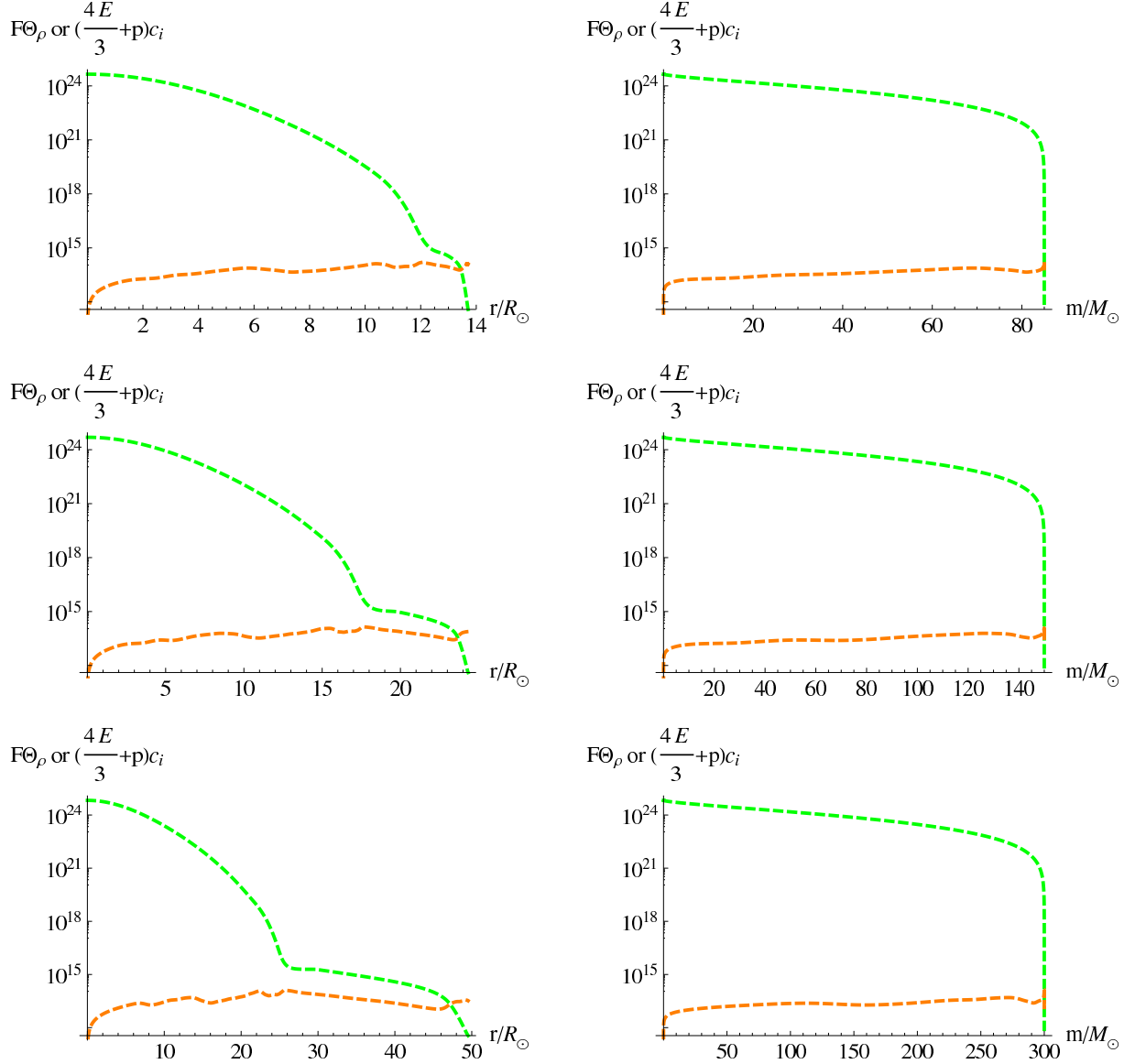
Fig. 4.— Radiative instabilities in the envolopes of massive stars. From the top row to the bottom row are stellar models of 85 $M_\odot$, 150 $M_\odot$ and 300 $M_\odot$, respectively. The orange dashed lines are related to the radiative flux $F\Theta_\rho$, and the green dashed lines represent the damping term $\left(\frac{4E}{3} + p\right) c_i$. The left panels are ploted in terms of the stellar radius, while the right panels are in terms of the stellar mass below that point.

REFERENCES

Blaes, O., & Socrates, A. 2003, ApJ, 596, 509

Crowther, P. A., Schnurr, O., Hirschi, R., Yusof, N., Parker, R. J., Goodwin, S. P., & Kassim, H. A. 2010, MNRAS, 408, 731

Damineli, A. 1996, ApJ, 460, L49

Davidson, K., & Humphreys, R. M. 1997, ARA&A, 35, 1

Eggleton, P. P. 1971, MNRAS, 151, 351

Figer, D. F. 2005, Nature, 434, 192

Iping, R. C., Sonneborn, G., Gull, T. R., Massa, D. L., & Hillier, D. J. 2005, ApJ, 633, L37

Kashi, A., & Soker, N. 2010, ApJ, 723, 602

Kippenhahn, R., & Weigert, A. 1994, Stellar Structure and Evolution, study edn. (Springer)

Krumholz, M. R., & Bonnell, I. A. 2009, Models for the formation of massive stars, ed. Chabrier, G. (Cambridge University Press), 288–320

Smith, N. 2010, ArXiv e-prints

Stancliffe, R. J., & Eldridge, J. J. 2009, MNRAS, 396, 1699

Vink, J. S. 2009, ArXiv e-prints